

Creation of Bifunctional Materials: Improve Electron-Transporting Ability of Light Emitters Based on AIE-Active 2,3,4,5-Tetraphenylsiloles

Long Chen, Yibin Jiang, Han Nie, Ping Lu, Herman H. Y. Sung, Ian D. Williams, Hoi Sing Kwok, Fei Huang, Anjun Qin, Zujin Zhao,* and Ben Zhong Tang*

2,3,4,5-Tetraphenylsiloles are excellent solid-state light emitters featured aggregation-induced emission (AIE) characteristics, but those that can efficiently function as both light-emitting and electron-transporting layers in one organic light-emitting diode (OLED) are much rare. To address this issue, herein, three tailored n-type light emitters comprised of 2,3,4,5-tetraphenylsilole and dimesitylboryl functional groups are designed and synthesized. The new siloles are fully characterized by standard spectroscopic and crystallographic methods with satisfactory results. Their thermal stabilities, electronic structures, photophysical properties, electrochemical behaviors and applications in OLEDs are investigated. These new siloles exhibit AIE characteristics with high emission efficiencies in solid films, and possess lower LUMO energy levels than their parents, 2,3,4,5-tetraphenylsiloles. The double-layer OLEDs [ITO/NPB (60 nm)/silole (60 nm)/LiF (1 nm)/Al (100 nm)] fabricated by adopting the new siloles as both light emitter and electron transporter afford excellent performances, with high electroluminescence efficiencies up to 13.9 cd A⁻¹, 4.35% and 11.6 lm W⁻¹, which are increased greatly relative to those attained from the triple-layer devices with an additional electron-transporting layer. These results demonstrate effective access to n-type solid-state emissive materials with practical utility.

1. Introduction

Organic luminescent materials have been the subject of intense academic and commercial interest over the past two decades because of their various practical applications such as light emitters for organic light-emitting diodes (OLEDs).^[1] Although considerable progresses have been made in the development of organic emitters, major challenges still remain. One stubborn problem is that many “conventional” luminophors that show good emissions in solutions suffer from aggregation-caused quenching (ACQ) in the condensed phase. This becomes one of the thorny obstacles to the evolution of OLEDs, for most light emitters have to be fabricated into solid films when used in devices.^[2] Various chemical, physical and engineering approaches have been proposed to mitigate the ACQ effect.^[3] But these methods often lead to some side effects, rendering efficient solid-state emitters infrequent. It will be nice, if a system can be developed,

in which light emission is enhanced rather than quenched by aggregation. In 2001, Tang's group found that 1-methyl-1,2,3,4,5-pentaphenylsilole (MPPS) was almost non-fluorescent in solution but it could emit strong light when aggregated in poor solvents or fabricated into solid films, demonstrating an intriguing phenomenon of aggregation-induced emission (AIE).^[4] Based on this finding, many AIE-active luminogens are developed, making pure solid films with high emission efficiencies readily achievable. This paves a new avenue to realize efficient non-doped OLEDs,^[2,5] which avoid the complicated and hard-to-control processes of the doping techniques used to alleviate the ACQ effect of light emitters.

Another challenge for next generation of high-performance OLEDs is to simplify device configuration and cut down the cost, without sacrificing device efficiency.^[6] In this regard, design and synthesis of new luminescent materials that can simultaneously serve as light emitter and hole-/electron-transporting material in one device is a promising alternative. Compared with organic hole-transporting (p-type) luminophors,^[7] electron-transporting (n-type) materials with low

L. Chen, H. Nie, Prof. F. Huang, Prof. A. Qin,
Prof. Z. Zhao, Prof. B. Z. Tang
State Key Laboratory of Luminescent
Materials and Devices
South China University of Technology
Guangzhou 510640, China
E-mail: zujinzhao@gmail.com; tangbenz@ust.hk

Y. Jiang, Prof. H. S. Kwok
Center for Display Research
The Hong Kong University of Science & Technology (HKUST)
Kowloon, Hong Kong, China

Dr. P. Lu
State Key Laboratory of Supramolecular Structure and Materials
Jilin University
Changchun 130012, China

Dr. H. H. Y. Sung, Prof. I. D. Williams, Prof. B. Z. Tang
Division of Biomedical Engineering
Department of Chemistry
Institute for Advanced Study and Institute
of Molecular Functional Materials
HKUST, Clear Water Bay
Kowloon, Hong Kong



DOI: 10.1002/adfm.201303867

electron injection barrier and fast electron mobility in addition to excellent solid-state emission are scarce.^[8]

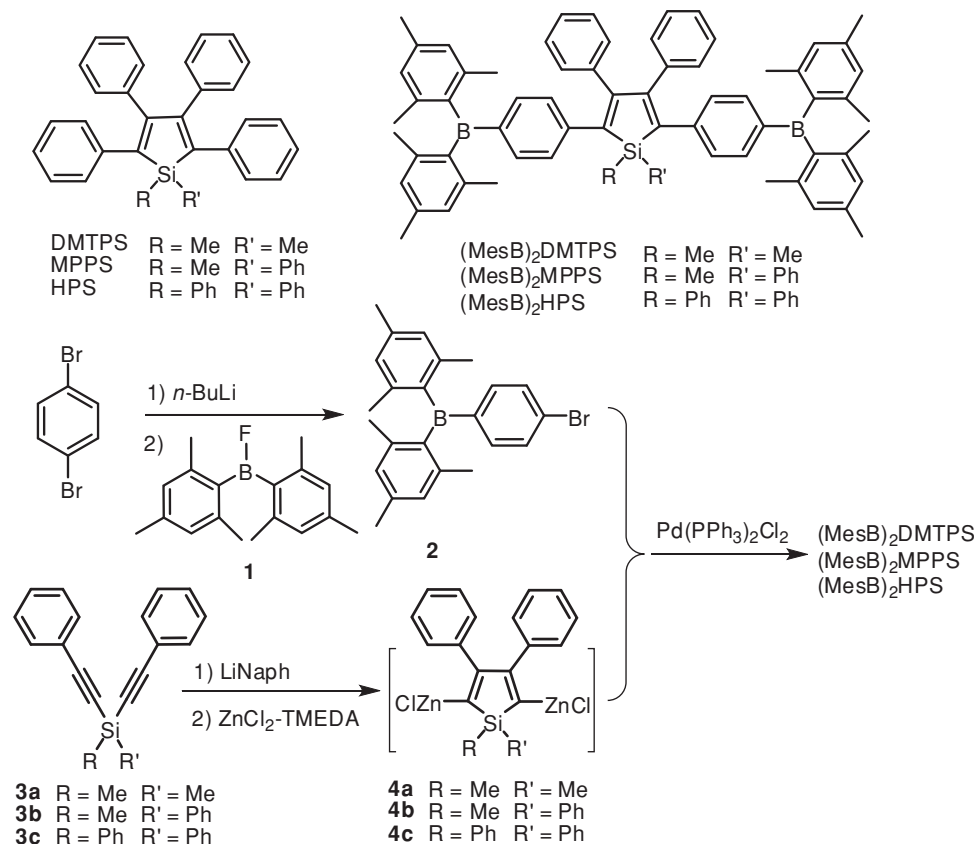
Among numerous AIE luminogens, siloles have attracted considerable attention because of not only bright emissions in solid films but also unique electronic structures.^[9] The effective $\sigma^*-\pi^*$ conjugation between the σ^* orbitals of two exocyclic silicon-carbon bonds and π^* orbital of the butadiene moiety imparts the low-lying lowest unoccupied molecular orbital (LUMO) and high electron affinity to siloles.^[10] So far, efficient solid-state emitters and electron transporter have been developed based on siloles.^[11] Multiple OLEDs utilizing two different kinds of silole derivatives as light-emitting and electron-transporting layers, respectively, had been tried by Kafafi et al., which afforded high efficiencies up to 4.1%.^[12] However, the combination of both merits of siloles to generate efficient n-type light emitters has been barely realized. In our previous studies, we found that OLEDs fabricated by using 2,3,4,5-tetraphenylsiloles (Scheme 1) as light-emitting layers afforded remarkably high electroluminescence (EL) efficiency.^[13] But these devices need an electron-transporting layer to balance the holes and electrons, implying that the 2,3,4,5-tetraphenylsiloles are excellent light emitters but their electron-transporting ability needs to be further enhanced. In view of this, three tailored silole derivatives consisting of 2,3,4,5-tetraphenylsiloles and bimesitylboryl groups are designed and synthesized in this work (Scheme 1). It is envisioned that the incorporation of inherently electron deficient group, dimesitylboryl, is beneficial to advances in

electron affinity and electron-transporting ability.^[14] The thermal, photophysical, electronic, electrochemical, and electro-luminescent properties of the new siloles are investigated. The results reveal that these new siloles are efficient bifunctional materials for OLEDs.

2. Results and Discussion

2.1. Synthesis

The target 2,3,4,5-tetraphenylsiloles carrying dimesitylboryl groups, (MesB)₂DMTPS, (MesB)₂MPPS and (MesB)₂HPS, were facily prepared according to the synthetic routes outlined in Scheme 1. The detailed procedures and characterization data are given in the Experimental section. Briefly, compounds 2^[15] and 3^[16] were prepared according to the methods described in the literature. The treatments of 3 with lithium 1-naphthalenide (LiNaph), and subsequent ZnCl₂-TMEDA generated 2,5-metallated silole intermediates (4). Without purification, 4 underwent coupling reaction with 2 in the presence of a palladium catalyst, affording final compounds (MesB)₂DMTPS, (MesB)₂MPPS and (MesB)₂HPS in 80, 50 and 40% yields, respectively. The new siloles were fully characterized by NMR and mass spectroscopies, which confirmed their molecular structures. They are soluble in common organic solvents including THF, dichloromethane, chloroform, toluene, etc., but insoluble in water.



Scheme 1. Synthetic routes to dimesitylboryl-functionalized 2,3,4,5-tetraphenylsiloles. LiNaph = lithium 1-naphthalenide; TMEDA = *N,N,N',N'*-tetramethylethylenediamine.

Table 1. Optical, electronic and thermal properties of (MesB)₂DMTPS, (MesB)₂MPPS and (MesB)₂HPS.

Compounds	λ_{ab} ^{a)} [nm]	λ_{em} ^{b)} (Φ_F ^{c)} [nm] (%)		T_g/T_d [°C]	HOMO/LUMO [eV]	E_g [eV]
		Soln (Φ_F)	Film (Φ_F)			
(MesB) ₂ DMTPS	392	512(0.87)	516(56)	121/240	-5.6/-3.0	2.6
(MesB) ₂ MPPS	395	516(1.35)	524(58)	131/269	-5.7/-3.1	2.6
(MesB) ₂ HPS	396	523(1.38)	526(62)	123/289	-5.7/-3.1	2.6

^{a)}Absorption maximum in dilute THF solution (10 μ M); ^{b)}Emission maximum in THF solution; ^{c)}Fluorescence quantum yield in THF solution (soln) determined using quinine sulfate ($\Phi_F = 54.6\%$ in 0.1 N sulfuric acid) as standard or in the film state by a calibrated integrating sphere.

The thermal properties of (MesB)₂DMTPS, (MesB)₂MPPS and (MesB)₂HPS were evaluated by thermogravimetric analysis (TGA) and differential scanning calorimetry (DSC). The results show that they possess good thermal stability with decomposition temperatures (T_d) of 240–289 °C, according to 5% loss of initial weight. High glass-transition temperatures (T_g) of 121–131 °C (Table 1) are recorded from the new siloles, indicating that they are morphologically stable. The good thermal and morphological stabilities enable them to serve as active materials for OLEDs.

2.2. Crystal Structure

Single crystals of (MesB)₂DMTPS and (MesB)₂HPS were grown from THF/ethanol mixture, and analyzed by X-ray diffraction crystallography. Figure 1 displays the crystal structures of (MesB)₂DMTPS and (MesB)₂HPS. It can be seen that in the crystalline state, both siloles show twisted conformations and no π - π stacking interactions are found between aromatic rings. Figure 2 illustrates the molecular packing patterns of (MesB)₂DMTPS and (MesB)₂HPS in the crystalline state. The (MesB)₂HPS molecules are arranged more regularly and tightly than (MesB)₂DMTPS molecules. The close packing of (MesB)₂HPS suggest that it should have better carrier-transporting ability than (MesB)₂DMTPS.

2.3. Optical Property

The absorption spectra of the new siloles in dilute THF solutions (10 μ M) are shown in Figure 3A. The spectral profiles of (MesB)₂DMTPS, (MesB)₂MPPS and (MesB)₂HPS are similar, with maxima at 392, 395, and 396 nm, respectively, associated to π - π^* transitions. The photoluminescence (PL) spectra of three siloles in dilute THF solutions (10 μ M) are shown in Figure 3B. Like most silole derivatives, these new siloles show weak emissions in

the solution state. Only faint PL signals peaked at 512, 516 and 523 nm are recorded for (MesB)₂DMTPS, (MesB)₂MPPS and (MesB)₂HPS, respectively. The fluorescence quantum yields (Φ_F) of (MesB)₂DMTPS, (MesB)₂MPPS, and (MesB)₂HPS in dilute THF solutions are as low as 0.87, 1.35, and 1.38%, respectively, estimated using quinine sulfate ($\Phi_F = 54.6\%$ in 0.1 N sulfuric acid) as standard, which indicates that they are practically very weak emitters when dissolved in good solvents. These siloles become highly emissive in the solid state. The films of (MesB)₂DMTPS, (MesB)₂MPPS, and (MesB)₂HPS

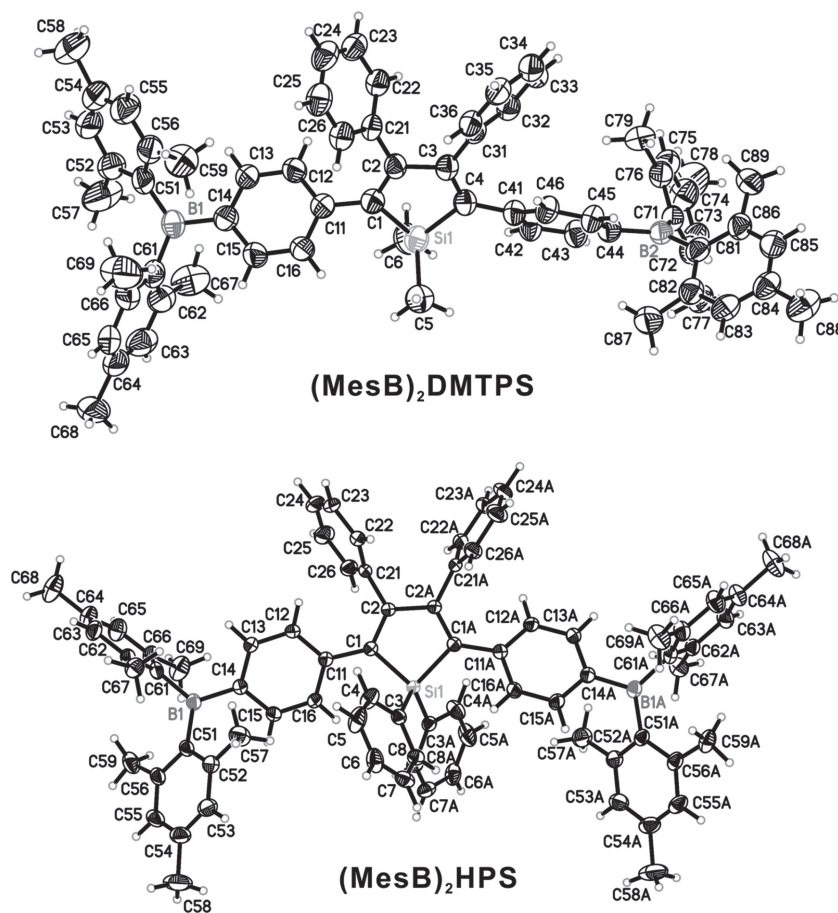


Figure 1. ORTEP drawings of (MesB)₂DMTPS (CCDC 948629) and (MesB)₂HPS (CCDC 948630).

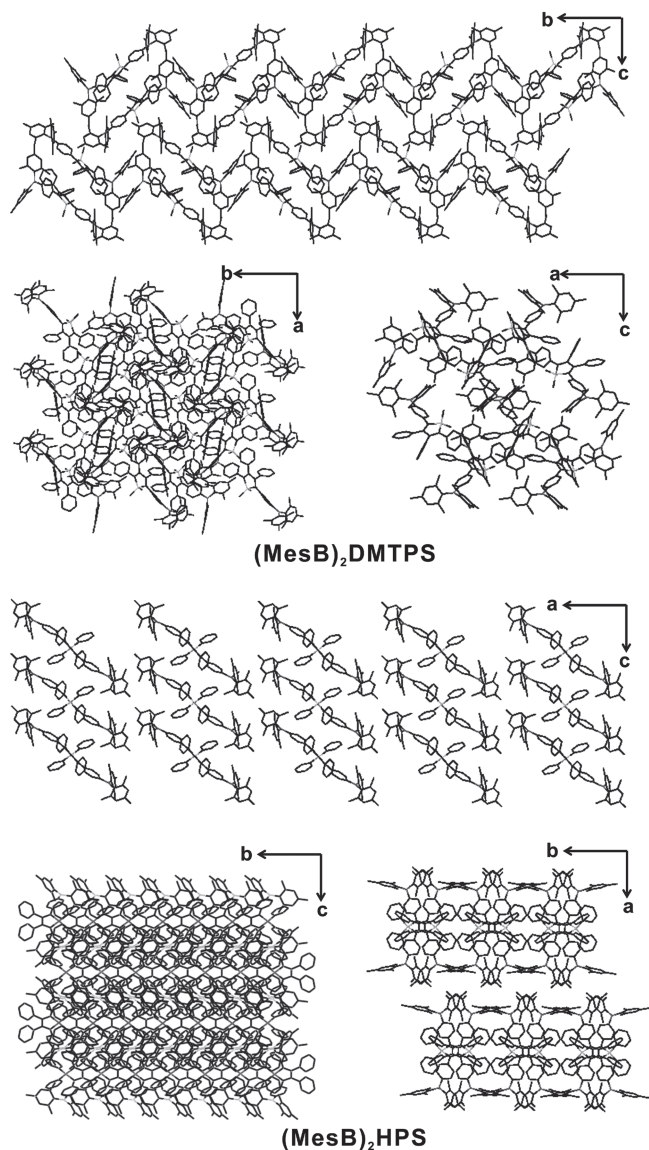


Figure 2. Molecular packing patterns of $(\text{MesB})_2\text{DMTPS}$ and $(\text{MesB})_2\text{HPS}$ in the crystalline state.

fluoresce intensely with emission maxima at 516, 524, and 526 nm, respectively (Figure S1, Supporting Information). Only slight bathochromic shifts are observed in the PL spectra of the films compared to those of the solutions, which is attributable to the propeller-like molecular conformations as well as the branched dimethylboryl groups that have impeded close π -stacking interactions. The Φ_F values of the films, determined by integrating sphere, are as high as 56, 58, and 62% for $(\text{MesB})_2\text{DMTPS}$, $(\text{MesB})_2\text{MPPS}$, and $(\text{MesB})_2\text{HPS}$, revealing that they are AIE-active and are excellent solid-state emitters.

The AIE attributes of the new siloles are further confirmed by their emission behaviors in THF/water mixtures. **Figure 4A** illustrates the PL spectra of $(\text{MesB})_2\text{MPPS}$ in THF/water mixtures as an example. It can be seen that when the water content is low, the emission is weak. But when the water content becomes high, the emission intensity enhances swiftly

(Figure 4B). Similar emission behaviors are also recorded from $(\text{MesB})_2\text{DMTPS}$ and $(\text{MesB})_2\text{HPS}$ in THF/water mixtures (Figure S2, Supporting Information). Since $(\text{MesB})_2\text{DMTPS}$, $(\text{MesB})_2\text{MPPS}$, and $(\text{MesB})_2\text{HPS}$ are insoluble in water, their molecules must have aggregated in aqueous medium. The intramolecular rotation that is active in the solution state is restricted due to steric hindrance in the condensed phase. The nonradiative relaxation channel is thus blocked and radiative decay of the excited state is promoted, rendering molecules highly emissive. These results manifest that the new siloles are AIE-active indeed.

2.4. Theoretical Calculation

To gain a deep insight into the electronic structures of the new siloles, theoretical calculations are performed by density function theory (DFT) method with a B3LYP/6-31G(d) basis set using Gaussian 09 package. The optimized structures and orbital distributions of the HOMOs and LUMOs of $(\text{MesB})_2\text{DMTPS}$, $(\text{MesB})_2\text{MPPS}$, and $(\text{MesB})_2\text{HPS}$ are shown in **Figure 5**. All the molecules adopt twisted conformations, which would hamper the strong intermolecular interactions between the molecules. In LUMOs, significant contributions from the boron centers are observed, owing to the $p\pi$ - π^* conjugation between empty $p\pi$ orbital of boron atom and π^* orbitals of the phenyl rings. Meanwhile, the electronic cloud of LUMOs can also delocalize to exocyclic Si-C bonds through σ^* - π^* conjugation. Such distinctive electronic structures result in low LUMO energy levels of -1.97 , -2.05 , and -2.04 eV for $(\text{MesB})_2\text{DMTPS}$, $(\text{MesB})_2\text{MPPS}$, and $(\text{MesB})_2\text{HPS}$, respectively. The values are much lower than those of DMTPS (-1.59 eV) and other 2,3,4,5-tetraphenylsiloles,^[17] demonstrating that the incorporation of dimethylboryl groups has effectively lowered the LUMO energy levels. The electron injection and transport become more favorable in the new siloles than their parents.

2.5. Electrochemical Property

The electrochemical properties of $(\text{MesB})_2\text{DMTPS}$, $(\text{MesB})_2\text{MPPS}$, and $(\text{MesB})_2\text{HPS}$ were investigated by cyclic voltammetry (CV) in dichloromethane solution with 0.1 M tetrabutylammonium hexafluorophosphate as the supporting electrolyte at a scan rate of 50 mV s^{-1} using platinum as the working electrode and saturated calomel electrode (SCE) as the reference electrode. The new siloles exhibit similar CV curves (**Figure 6**). The oxidation onset potentials (E_{onset}) of $(\text{MesB})_2\text{DMTPS}$, $(\text{MesB})_2\text{MPPS}$, and $(\text{MesB})_2\text{HPS}$ occur at 1.2, 1.3, and 1.3 V, respectively. The energy levels of HOMO [$\text{HOMO} = -(4.4 + E_{\text{onset}})$] and LUMO [$\text{LUMO} = -(\text{HOMO} + E_g)$] were determined by E_{onset} and optical band gaps. The HOMO energy levels are calculated to be -5.6 , -5.7 , and -5.7 eV, and the LUMO energy levels are -3.0 , -3.1 , and -3.1 eV for $(\text{MesB})_2\text{DMTPS}$, $(\text{MesB})_2\text{MPPS}$, and $(\text{MesB})_2\text{HPS}$, respectively. The LUMO energy levels of the present siloles are equal to or even lower than those of widely used electron-transporting materials, for example, tris(8-hydroxyquinoline) aluminum (Alq_3 , -3.0 eV) and 1,3,5-tris(*N*-phenylbenzimidazol-2-yl)benzene

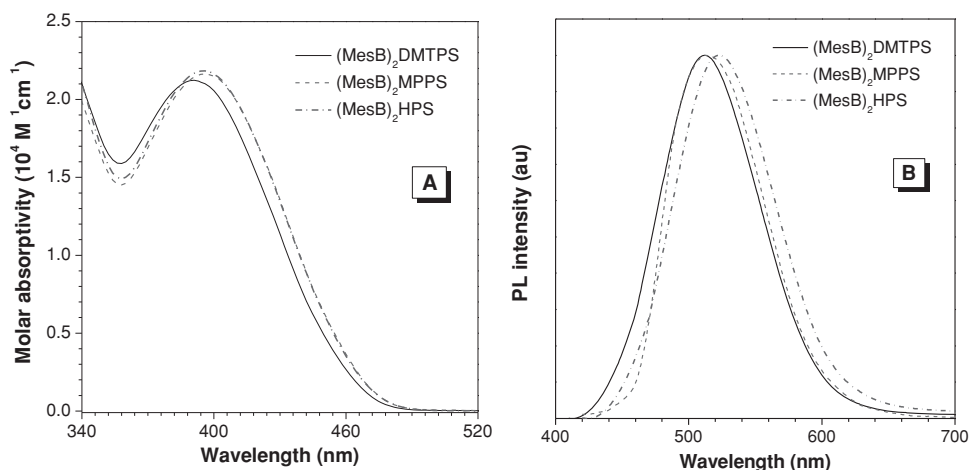


Figure 3. A) Absorption and B) PL spectra of (MesB)₂DMTPS, (MesB)₂MPPS, and (MesB)₂HPS in THF solutions (10 μM). Excitation wavelength: 380 nm.

(TPBi, -2.7 eV), indicating their great potential as electron-transporting materials for OLEDs.

2.6. Electroluminescence

The efficient solid-state PL emissions of (MesB)₂DMTPS, (MesB)₂MPPS, and (MesB)₂HPS inspire us to evaluate their electroluminescence (EL) properties in non-doped OLEDs. Triple-layer OLEDs with a configuration of ITO/NPB (60 nm)/silole (20 nm)/TPBi (40 nm)/LiF (1 nm)/Al (100 nm) (Device I) are fabricated, in which (MesB)₂DMTPS, (MesB)₂MPPS or (MesB)₂HPS serve as light-emitting layer (EML), *N,N'*-di(1-naphthyl)-*N,N'*-diphenyl-benzidine (NPB) acts as hole-transporting layer (HTL) and TPBi functions as electron-transporting layer (ETL). The devices I of the new siloles radiate yellow lights, whereas the PL emissions of the films are in the green region. Taking (MesB)₂MPPS as an example, its EL maximum

is located at 552 nm, which is red-shifted by 28 nm in comparison with its PL in film (Figure 7A). Such kind of red shifts could be ascribed to space charge accumulation caused by the imbalance of charge transport.^[18] The performances of devices I summarized in Table 2 are moderate and the turn-on voltages are relatively high. These results indicate that the standard device configuration with three active layers may not suitable for the present siloles.

Considering the low-lying LUMO energy levels of the new siloles, it is envisioned that they may function as electron transporter in addition to light emitter in device. To confirm this, double-layer OLEDs with a configuration of ITO/NPB (60 nm)/silole (60 nm)/LiF (1 nm)/Al (100 nm) (Device II) are fabricated, in which (MesB)₂DMTPS, (MesB)₂MPPS, or (MesB)₂HPS serve as both EML and ETL, and NPB acts as HTL. Devices II of (MesB)₂MPPS and (MesB)₂HPS exhibit similar EL emissions to the PL emissions of films. For instance, the EL spectrum of (MesB)₂MPPS with a peak at 520 nm is almost identical to the

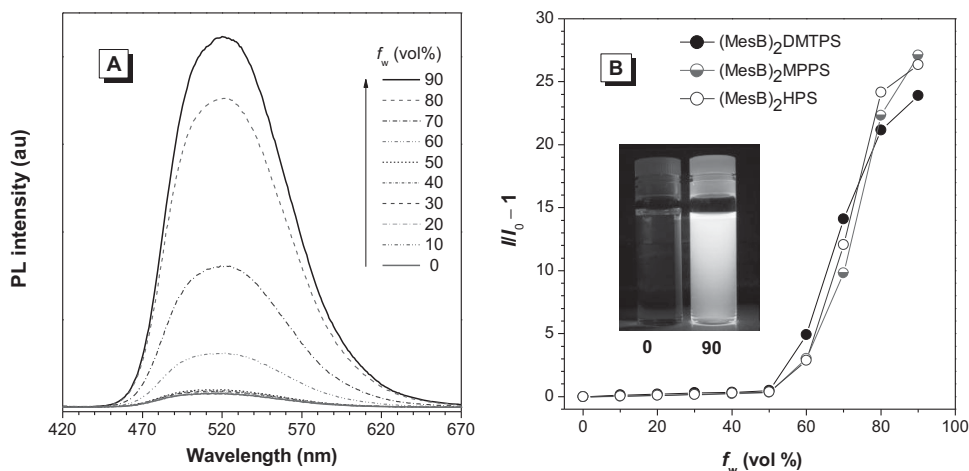


Figure 4. A) PL spectra of (MesB)₂MPPS in THF/water mixtures with different water fractions (f_w). B) Plot of $(I/I_0 - 1)$ values versus water fractions in THF/water mixtures of (MesB)₂DMTPS, (MesB)₂MPPS, and (MesB)₂HPS. I_0 is the PL intensity in pure THF solution. Inset: photos of (MesB)₂MPPS in THF/water mixtures ($f_w = 0$ and 90%), taken under the illumination of a UV lamp.

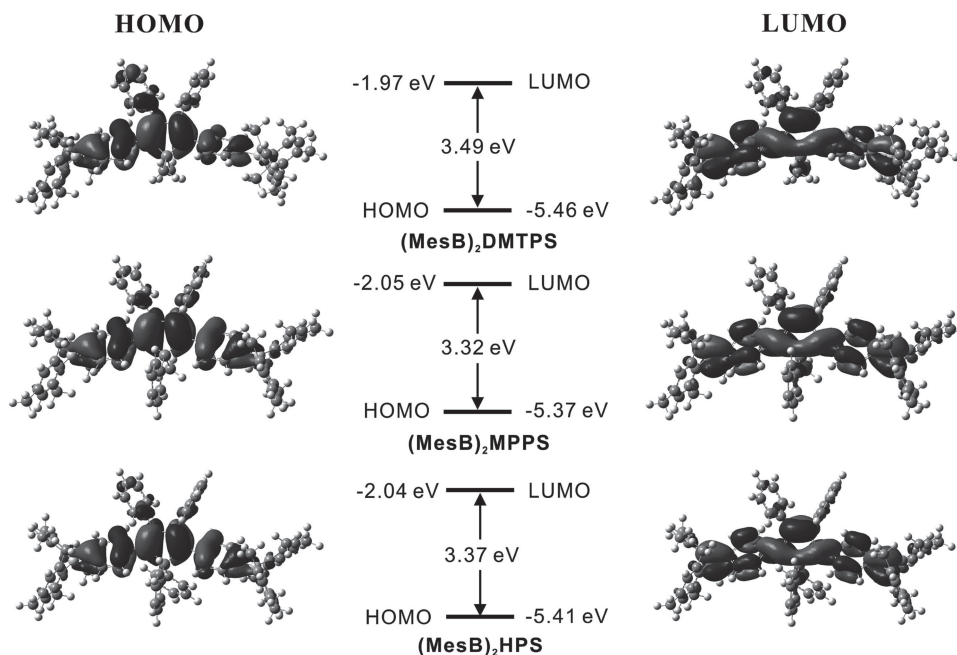


Figure 5. B3LYP/6–31G(d) calculated molecular orbital amplitude plots and energy levels of HOMOs and LUMOs of $(\text{MesB})_2\text{DMTPS}$, $(\text{MesB})_2\text{MPPS}$, and $(\text{MesB})_2\text{HPS}$.

PL spectrum of film (524 nm) (Figure 7A), indicating that the holes and electrons get more balanced, and the exciton recombination zone has been confined inside the silole layer.

The device II adopting $(\text{MesB})_2\text{MPPS}$ as both EML and ETL is turned on at a much lower voltage (3.9 V) than its device I with TPBi as ETL (7.5 V). It also shows higher current densities, and better luminance at the same voltages than device I (Figure 7B). The maximum luminance (L_{max}) of device II is 13 900 cd m^{-2} , which is higher than that of device I (9610 cd m^{-2}). Figure 7C,D depict the current efficiency and external quantum efficiency as a function of luminance for both devices I and II of $(\text{MesB})_2\text{MPPS}$. It can be seen that both efficiencies of device II

are advanced noticeably. Excellent maximum current (η_{C}), and external quantum (η_{ext}) efficiencies of 13.0 cd A^{-1} , and 4.12%, respectively, are attained by device II, which are almost twice as much as those of device I (6.6 cd A^{-1} , and 2.13%). The maximum power efficiency (η_{p}) of device II reaches 10.5 lm W^{-1} , being about four-fold higher than that of device I (2.4 lm W^{-1}). Significantly, device II shows a small roll-off in EL efficiencies when luminance increases, and a high current efficiency of 7.0 cd A^{-1} is reserved at a luminance of 1000 cd m^{-2} . This is very important because the lack of a hole-blocking layer often causes a large efficiency roll-off at high luminance range. Similarly, device II of $(\text{MesB})_2\text{HPS}$ also shows better performances than device I. The turn-on voltage of device II is decreased (4.3 vs. 5.4 V), and the peak EL efficiencies are enhanced obviously (η_{C} , 13.9 vs 8.4 cd A^{-1} ; η_{ext} , 4.35 vs 2.62%; η_{p} , 11.6 vs 4.1 lm W^{-1}) (Table 2 and Supporting Information Figure S3). These values are much better than those obtained from double-layer OLEDs of the reported n-type light emitters with close emission colors, such as copolymers of silafluorene and 2,1,3-benzothiadiazole (10.6 cd A^{-1} ; 3.81%),^[19] folded tetraphenylethene derivatives (7.9 cd A^{-1} ; 3.1%),^[5b] dimesitylboryl-functionalized tetraphenylethene (7.13 cd A^{-1} ; 2.7%),^[20] cyano-substituted pyridine derivatives (5.4 cd A^{-1}),^[21] Alq₃ (3.3 cd A^{-1}),^[22] spiro-bisilole derivatives (1.98 cd A^{-1}),^[23] and so forth.

Since both $(\text{MesB})_2\text{MPPS}$ and $(\text{MesB})_2\text{HPS}$ have closer LUMO energy levels to that of LiF/Al, the electron-injection is more favorable from LiF/Al to $(\text{MesB})_2\text{MPPS}$ and $(\text{MesB})_2\text{HPS}$ than to TPBi (Figure 8). The TPBi layer is virtually not necessary. It may even cause adverse effect to device performances because of the contact resistance at the interfaces. In addition, the excellent electron-transporting ability stemmed from the synergistic effect of silole ring and boron atoms leads to the shift of the current density-voltage characteristics to lower

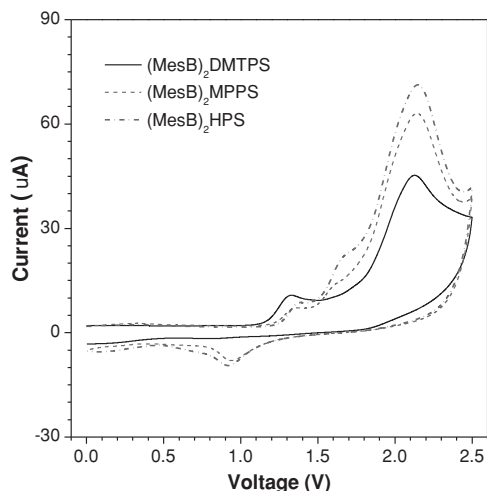


Figure 6. Cyclic voltammograms of $(\text{MesB})_2\text{DMTPS}$, $(\text{MesB})_2\text{MPPS}$, and $(\text{MesB})_2\text{HPS}$, measured in dichloromethane containing 0.1 M tetra-*n*-butylammonium hexafluorophosphate. Scant rate: 50 mV s^{-1} .

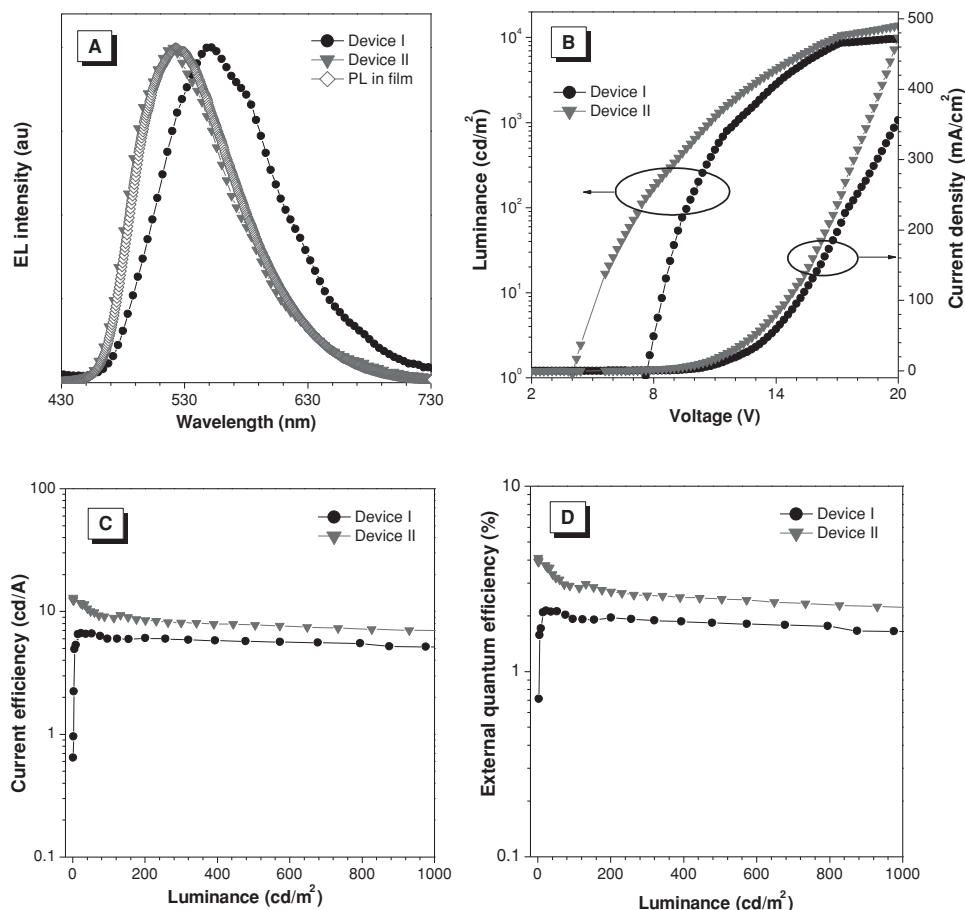


Figure 7. A) PL and EL spectra of solid thin film of $(\text{MesB})_2\text{MPPS}$. B) Current density-voltage-luminance characteristics, and C) current and D) external quantum efficiencies with the luminance in EL devices of $(\text{MesB})_2\text{MPPS}$. Device configuration: ITO/NPB (60 nm)/ $(\text{MesB})_2\text{MPPS}$ (20 nm)/TPBi (40 nm)/LiF (1 nm)/Al (100 nm) (Device I); ITO/NPB (60 nm)/ $(\text{MesB})_2\text{MPPS}$ (60 nm)/LiF (1 nm)/Al (100 nm) (Device II).

voltages. At the same time, electron accumulation and exciton quenching at the cathode are reduced. The balance of holes and electrons is improved, and thus the carrier recombination probability is increased, leading to advance in EL performances.

The current and external quantum efficiencies of device II of $(\text{MesB})_2\text{DMTPS}$ are increased slightly relative to those of device

I (Table 2, Figure S4, Supporting Information). However, the turn-on voltage is increased and the luminance is decreased. Since electron-transporting ability is not dependent solely on the energy levels of the materials, the arrangement of the molecules in solid film also functions as a crucial factor. Close packing of molecules is conducive to the carrier transport. From crystalline

Table 2. EL performances of OLEDs based on $(\text{MesB})_2\text{DMTPS}$, $(\text{MesB})_2\text{MPPS}$, and $(\text{MesB})_2\text{HPS}$. Abbreviations: λ_{EL} = electroluminescence maximum, V_{on} = turn-on voltage at 1 cd m^{-2} , L_{max} = maximum luminance, η_{c} = maximum current efficiency, η_{ext} = maximum external quantum efficiency, η_{p} = maximum power efficiency, CIE = Commission Internationale de l'Éclairage coordinates.

Emitter	Device ^{a)}	λ_{EL} [nm]	V_{on} [V]	L_{max} [cd m^{-2}]	η_{c} [cd A^{-1}]	η_{ext} [%]	η_{p} [lm W^{-1}]	CIE (x, y)
$(\text{MesB})_2\text{DMTPS}$	I	540	6.9	10500	7.4	2.25	3.2	0.35, 0.55
	II	536	6.9	1810	7.8	2.35	2.3	0.35, 0.57
$(\text{MesB})_2\text{MPPS}$	I	552	7.5	9610	6.6	2.13	2.4	0.40, 0.54
	II	520	3.9	13900	13.0	4.12	10.5	0.30, 0.56
$(\text{MesB})_2\text{HPS}$	I	548	5.4	15200	8.4	2.62	4.1	0.39, 0.55
	II	524	4.3	12200	13.9	4.35	11.6	0.33, 0.56

^{a)}Device configuration: ITO/NPB (60 nm)/silole (20 nm)/TPBi (40 nm)/LiF (1 nm)/Al (100 nm) (Device I); ITO/NPB (60 nm)/silole (60 nm)/LiF (1 nm)/Al (100 nm) (Device II).

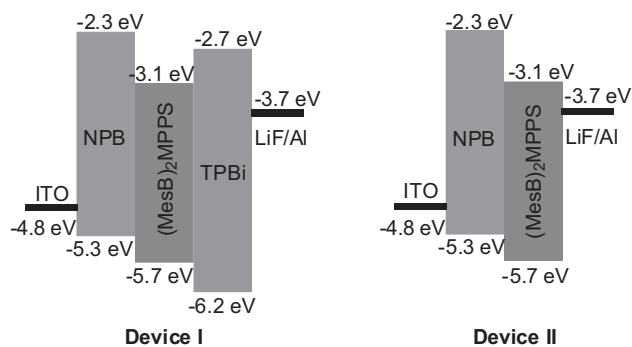


Figure 8. Energy level diagrams of multilayer EL devices of $(\text{MesB})_2\text{MPPS}$ with or without TPBi as electron-transporting layer.

geometry illustrated in Figure 2, we can see that $(\text{MesB})_2\text{HPS}$ molecules adopt a much tighter packing manner than $(\text{MesB})_2\text{DMTPS}$. Thereby, it is highly possible that $(\text{MesB})_2\text{HPS}$ molecules could pile up more closely than $(\text{MesB})_2\text{DMTPS}$ molecule even in amorphous films. This renders easier electron injection and better electron transport, and hence, superior EL property of $(\text{MesB})_2\text{HPS}$ to $(\text{MesB})_2\text{DMTPS}$. It should also be noted that the devices have not yet been optimized thoroughly. Many factors, for example, cathode materials, carrier injection layers, hole-transporting layers, the layer thicknesses, and substrate temperature for film deposition, have subtle impacts on the balance of carrier injection, carrier mobility, carrier recombination zone and efficiency, and so on. Therefore, given the excellent optoelectronic property of the new siloles, more efficient OLEDs are expectable via device engineering.

3. Conclusions

In summary, three thermally stable 2,3,4,5-tetraphenylsiloles modified with dimesitylboryl groups are synthesized, and their molecular structures and arrangement in the crystalline state are investigated. The new siloles are weakly fluorescent in solutions but become highly emissive in the aggregate state, presenting AIE characteristics. Thanks to the synergistic effect between silole ring and dimesitylboryl groups, the LUMO energy levels of the new siloles are lowered and the electron-transporting ability is improved. These merits enable them to serve simultaneously as bifunctional materials of light emitter and electron transporter in OLEDs. Efficient double-layer devices are achieved based on them, exhibiting greatly enhanced performances relative to triple-layer devices with these siloles as light emitters and TPBi as electron transporter. To the best of our knowledge, $(\text{MesB})_2\text{MPPS}$ and $(\text{MesB})_2\text{HPS}$ are among the best n-type luminescent materials used in the non-doped OLEDs. These results demonstrate an effective molecular design approach to bifunctional candidates (n-type light emitters) for OLEDs, for the sake of simplifying device configuration and reducing manufacturing cost.

4. Experimental Section

Materials and Instruments: THF was distilled from sodium benzophenone ketyl under dry nitrogen immediately prior to use. All

other chemicals and reagents were purchased from Aldrich and J&K Scientific Ltd., and used as received without further purification. ^1H and ^{13}C NMR spectra were measured on a Bruker AV 400 or AV 300 spectrometer in deuterated dichloromethane or chloroform using tetramethylsilane (TMS; $\delta = 0$) as internal reference. UV spectra were measured on a Milton Roy Spectronic 3000 Array spectrophotometer. PL spectra were recorded on a Perkin-Elmer LS 55 spectrofluorometer. High resolution mass spectra (HRMS) were recorded on a GCT premier CAB048 mass spectrometer operating in MALDI-TOF mode. Single crystal X-ray diffraction intensity data were collected on a Bruker-Nonices Smart Apex CCD diffractometer with graphite monochromated $\text{Mo K}\alpha$ radiation. Processing of the intensity data was carried out using the SAINT and SADABS routines, and the structure and refinement were conducted using the SHELTL suite of X-ray programs (version 6.10). TGA analysis was carried on a TA TGA Q5000 under dry nitrogen at a heating rate of $10\text{ }^\circ\text{C min}^{-1}$. The ground-state geometries were optimized using the density functional with B3LYP hybrid functional at the basis set level of 6-31G(d). All the calculations were performed using Gaussian 09 package.

Devices Fabrication: The devices were fabricated on 80 nm-ITO coated glass with a sheet resistance of $25\ \Omega\ \square^{-1}$. Prior to loading into the pretreatment chamber, the ITO-coated glass was soaked in ultrasonic detergent for 30 min, followed by spraying with de-ionized water for 10 min, soaking in ultrasonic de-ionized water for 30 min, and oven-baking for 1 h. The cleaned samples were treated by perfluoromethane plasma with a power of 100 W, gas flow of 50 sccm, and pressure of 0.2 Torr for 10 s in the pretreatment chamber. The samples were transferred to the organic chamber with a base pressure of 7×10^{-7} Torr for the deposition of NPB, emitter (and TPBi), which served as hole-transport, light-emitting (and electron-transport) layers, respectively. The samples were then transferred to the metal chamber for cathode deposition which composed of lithium fluoride (LiF) capped with aluminum (Al). The light-emitting area was $4\ \text{mm}^2$. The current density-voltage characteristics of the devices were measured by a HP4145B semiconductor parameter analyzer. The forward direction photons emitted from the devices were detected by a calibrated UDT PIN-25D silicon photodiode. The luminance and external quantum efficiencies of the devices were inferred from the photocurrent of the photodiode. The electroluminescence spectra were obtained by a PR650 spectrophotometer. All measurements were carried out under air at room temperature without device encapsulation.

Preparation of Nanoaggregates: Stock THF solutions of the siloles with a concentration of $10^{-4}\ \text{M}$ were prepared. Aliquots of the stock solution were transferred to 10 mL volumetric flasks. After appropriate amounts of THF were added, water was added dropwise under vigorous stirring to furnish $10^{-5}\ \text{M}$ solutions with different water contents (0–90 vol%). The PL measurements of the resultant solutions were then performed immediately.

Synthesis of 2,5-Bis(4-(dimesitylboryl)phenyl)-1,1-dimethyl-3,4-diphenylsilole ((MesB)₂DMTPS): A solution of lithium 1-naphthalenide (LiNaph) was prepared by stirring a mixture of naphthalene (2.56 g, 20 mmol) and lithium granular (0.14 g, 20 mmol) in dry THF (30 mL) for 4 h at room temperature under nitrogen. A solution of **3** (1.3 g, 5 mmol) in THF (20 mL) was then added dropwise into the solution of LiNaph, and the resultant mixture was stirred for 30 min at room temperature. The solution was cooled to $-10\text{ }^\circ\text{C}$, into which $\text{ZnCl}_2\text{-TMEDA}$ (6.3 g, 25 mmol) and 20 mL of THF were added. After the fine suspension was stirred for 1 h, $\text{Pd}(\text{PPh}_3)_2\text{Cl}_2$ (100 mg) and a solution of **2** (4.04 g, 10 mmol) in 10 mL THF were added. After reflux for 12 h, the reaction was cooled to room temperature and terminated by addition of 2 M hydrochloric acid. The mixture was poured into water and extracted with dichloromethane. The organic layer was washed successively with aqueous sodium chloride solution and water and then dried over magnesium sulfate. After filtration, the solvent was evaporated under reduced pressure and the residue was purified by silica-gel column chromatography using hexane as eluent. Recrystallization gave a yellow solid of product in ~80% yield. ^1H NMR (400 MHz, CD_2Cl_2), δ (ppm): 7.20 (d, $J = 8.0\ \text{Hz}$, 4H), 7.04–6.95 (m, 6H), 6.89 (d, $J = 8.0\ \text{Hz}$, 4H), 6.81–6.79 (m, 12H), 2.27 (s, 12H), 1.95 (s, 24H), 0.47 (s, 6H). ^{13}C

NMR (75 MHz, CDCl₃), δ (ppm): 155.0, 144.0, 143.0, 142.6, 141.8, 140.8, 138.5, 138.3, 136.3, 129.9, 128.3, 128.0, 127.3, 126.4, 23.3, 21.2, -3.9. HRMS (MALDI-TOF): m/z 910.5288 [M⁺, calcd 910.5276].

Synthesis of 2,5-Bis(4-(dimethylboryl)phenyl)-1-methyl-1,3,4-triphenylsilole ((MesB)₂MPPS): The procedure was analogous to that described for (MesB)₂DMTPS. Yellow solid; yield 50%. ¹H NMR (400 MHz, CD₂Cl₂), δ (ppm): 7.65 (d, J = 8.0 Hz, 2H), 7.38–7.30 (m, 3H), 7.10 (d, J = 8.0 Hz, 4H), 7.07–6.98 (m, 6H), 6.87 (d, J = 8.0 Hz, 4H), 6.82 (d, J = 8.0 Hz, 4H), 6.76 (s, 8H), 2.24 (s, 12H), 1.90 (s, 24H), 0.80 (s, 3H). ¹³C NMR (100 MHz, CDCl₃), δ (ppm): 156.5, 143.5, 143.0, 141.8, 141.3, 140.7, 138.6, 138.3, 136.2, 134.6, 133.2, 129.9, 128.5, 128.2, 128.0, 127.4, 126.6, 23.3, 21.2, -6.3. HRMS (MALDI-TOF): m/z 972.5442 [M⁺, calcd 972.5433].

Synthesis of 2,5-Bis(4-(dimethylboryl)phenyl)-1,1,3,4-tetraphenylsilole ((MesB)₂HPS): The procedure was analogous to that described for (MesB)₂DMTPS. Yellow solid; yield 40%. ¹H NMR (400 MHz, CD₂Cl₂), δ (ppm): 7.64 (d, J = 8.0 Hz, 4H), 7.45–7.42 (m, 2H), 7.35–7.32 (m, 4H), 7.08 (d, J = 8.0 Hz, 4H), 7.06–7.00 (m, 6H), 6.92 (d, J = 8.0 Hz, 4H), 6.86 (d, J = 8.0 Hz, 4H), 6.75 (s, 8H), 2.25 (s, 12H), 1.89 (s, 24H). ¹³C NMR (75 MHz, CDCl₃), δ (ppm): 157.6, 143.8, 143.3, 141.8, 140.8, 140.4, 138.6, 138.3, 136.0, 131.5, 130.2, 130.0, 128.8, 128.2, 128.0, 127.4, 126.6, 23.3, 21.2. HRMS (MALDI-TOF): m/z 1034.5597 [M⁺, calcd 1034.5589].

X-Ray Crystallography: Crystal data for (MesB)₂DMTPS (CCDC 948629): C₆₆H₆₈B₂Si, MW = 910.91, orthorhombic, P2(1)2(1)2(1), a = 12.0690(3), b = 17.7421(5), c = 26.1832(7) Å, V = 5606.6(3) Å³, Z = 4, D_c = 1.079 g cm⁻³, μ = 0.644 mm⁻¹ (MoK α , λ = 1.5418), $F(000)$ = 1952, T = 173.00(14) K, $2\theta_{\max}$ = 66.50° (99.36%), 32045 measured reflections, 9924 independent reflections (R_{int} = 0.0702), GOF on F^2 = 1.002, R_1 = 0.0903, wR_2 = 0.1230 (all data), $\Delta\rho$ 0.206 and -0.185 eÅ⁻³. Crystal data for (MesB)₂HPS (CCDC 948630): C₇₆H₇₂B₂Si, MW = 1035.05, monoclinic, C2/c, a = 37.0234(15), b = 10.5134(4), c = 15.9686(6) Å, β = 90.774(4)°, V = 6215.1(4) Å³, Z = 4, D_c = 1.106 g cm⁻³, μ = 0.639 mm⁻¹ (MoK α , λ = 1.5418), $F(000)$ = 2208, T = 173.00(14) K, $2\theta_{\max}$ = 66.50° (95.3%), 17 100 measured reflections, 5275 independent reflections (R_{int} = 0.0676), GOF on F^2 = 1.005, R_1 = 0.0764, wR_2 = 0.1531 (all data), $\Delta\rho$ 0.454 and -0.262 eÅ⁻³.

Supporting Information

Supporting Information is available from the Wiley Online Library or from the author.

Acknowledgements

The authors acknowledge the financial support from the National Natural Science Foundation of China (21104012 and 51273053), the National Basic Research Program of China (973 Program, 2013CB834702), the Fundamental Research Funds for the Central Universities (2013ZZ0002), the Guangdong Innovative Research Team Program of China (20110C0105067115) and the Research Grants Council of Hong Kong (HKUST2/CRF/10).

Received: November 14, 2013

Revised: December 18, 2013

Published online:

- [1] a) C. Tang, S. VanSlyke, *Appl. Phys. Lett.* **1987**, *51*, 913; b) A. C. Grimdsdale, K. Leok Chan, R. E. Martin, P. G. Jokisz, A. B. Holmes, *Chem. Rev.* **2009**, *109*, 897.
[2] a) Y. Hong, J. W. Y. Lam, B. Z. Tang, *Chem. Commun.* **2009**, 4332; b) Y. Hong, J. W. Y. Lam, B. Z. Tang, *Chem. Soc. Rev.* **2011**, *40*, 5361.
[3] a) P. N. Taylor, M. J. O'Connell, L. A. McNeill, M. J. Hall, R. T. Aplin, H. L. Anderson, *Angew. Chem. Int. Ed.* **2000**, *39*, 3456; b) L. Chen,

- S. Xu, D. McBranch, D. Whitten, *J. Am. Chem. Soc.* **2000**, *122*, 9302; c) S. Hecht, J. M. Fréchet, *Angew. Chem. Int. Ed.* **2001**, *40*, 74.
[4] J. Luo, Z. Xie, J. W. Y. Lam, L. Cheng, H. Chen, C. Qiu, H. S. Kwok, X. Zhan, Y. Liu, D. Zhu, B. Z. Tang, *Chem. Commun.* **2001**, 1740.
[5] a) Z. Zhao, J. W. Y. Lam, B. Z. Tang, *J. Mater. Chem.* **2012**, *22*, 23726; b) Z. Zhao, J. W. Y. Lam, C. Y. K. Chan, S. Chen, J. Liu, P. Lu, M. Rodriguez, J.-L. Maldonado, G. Ramos-Ortiz, H. H. Y. Sung, I. D. Williams, H. Su, K. S. Wong, Y. Ma, H. S. Kwok, H. Qiu, B. Z. Tang, *Adv. Mater.* **2011**, *23*, 5430; c) J. Mei, J. Wang, J. Z. Sun, H. Zhao, W. Yuan, C. Deng, S. Chen, H. H. Y. Sung, P. Lu, A. Qin, H. S. Kwok, Y. Ma, I. D. Williams, B. Z. Tang, *Chem. Sci.* **2012**, *3*, 549.
[6] a) W. L. Jia, X. D. Feng, D. R. Bai, Z. H. Lu, S. Wang, G. Vamvounis, *Chem. Mater.* **2004**, *17*, 164; b) L. Duan, J. Qiao, Y. Sun, Y. Qiu, *Adv. Mater.* **2011**, *23*, 1137.
[7] a) J. Y. Kim, T. Yasuda, Y. S. Yang, C. Adachi, *Adv. Mater.* **2013**, *25*, 2666; b) Z. Zhao, C. Y. K. Chan, S. Chen, C. Deng, J. W. Y. Lam, C. K. W. Jim, Y. Hong, P. Lu, Z. Chang, X. Chen, P. Lu, H. S. Kwok, H. Qiu, B. Z. Tang, *J. Mater. Chem.* **2012**, *22*, 4527; c) W. Z. Yuan, P. Lu, S. Chen, J. W. Y. Lam, Z. Wang, Y. Liu, H. S. Kwok, Y. Ma, B. Z. Tang, *Adv. Mater.* **2010**, *22*, 2159; d) W. Z. Yuan, Y. Gong, S. Chen, X. Y. Shen, J. W. Y. Lam, P. Lu, Y. Lu, Z. Wang, R. Hu, N. Xie, H. S. Kwok, Y. Zhang, J. Z. Sun, B. Z. Tang, *Chem. Mater.* **2012**, *24*, 1518.
[8] a) G. Hughes, M. R. Bryce, *J. Mater. Chem.* **2005**, *15*, 94; b) A. P. Kulkarni, C. J. Tonzola, A. Babel, S. A. Jenekhe, *Chem. Mater.* **2004**, *16*, 4556; c) J. E. Anthony, A. Facchetti, M. Heeney, S. R. Marder, X. Zhan, *Adv. Mater.* **2010**, *22*, 3876; d) J. Huang, X. Yang, X. Li, P. Chen, R. Tang, F. Li, P. Lu, Y. Ma, L. Wang, J. Qin, Q. Li, Z. Li, *Chem. Commun.* **2012**, *48*, 9586.
[9] a) B. Wrackmeyer, G. Kehr, J. Suss, E. Molla, *J. Organomet. Chem.* **1999**, *577*, 82; b) S. Yamaguchi, T. Endo, M. Uchida, T. Izumizawa, K. Furukawa, K. Tamao, *Chem. Eur. J.* **2000**, *6*, 1683; c) J. Ohshita, H. Kai, A. Takata, T. Iida, A. Kunai, N. Ohta, K. Komaguchi, M. Shiotani, A. Adachi, K. Sakamaki, K. Okita, *Organometallics* **2001**, *20*, 4800; d) J. W. Chen, C. C. W. Law, J. W. Y. Lam, Y. P. Dong, S. M. F. Lo, I. D. Williams, D. B. Zhu, B. Z. Tang, *Chem. Mater.* **2003**, *15*, 1535; e) A. J. Boydston, Y. Yin, B. L. Pagenkopf, *J. Am. Chem. Soc.* **2004**, *126*, 3724; f) L. Aubouy, P. Gerbier, N. Huby, G. Wantz, L. Vignau, L. Hirsch, J.-M. Janot, *New J. Chem.* **2004**, *28*, 1086; g) S. J. Toal, K. A. Jones, D. Magde, W. C. Trogler, *J. Am. Chem. Soc.* **2005**, *127*, 11661; h) S. H. Lee, B. B. Jang, Z. H. Kafafi, *J. Am. Chem. Soc.* **2005**, *127*, 9071; i) H. J. Tracy, J. L. Mullin, W. T. Klooster, J. A. Martin, J. Haug, S. Wallace, I. Rudloe, K. Watts, *Inorg. Chem.* **2005**, *44*, 2003; j) M. Wang, G. X. Zhang, D. Q. Zhang, D. B. Zhu, B. Tang, *J. Mater. Chem.* **2010**, *20*, 1858.
[10] a) X. Zhan, S. Barlow, S. R. Marder, *Chem. Commun.* **2009**, 1948; b) Z. Zhao, D. Liu, F. Mahtab, L. Xin, Z. Shen, Y. Yu, C. Y. K. Chan, P. Lu, J. W. Y. Lam, H. H. Y. Sung, I. D. Williams, B. Yang, Y. Ma, B. Z. Tang, *Chem. Eur. J.* **2011**, *17*, 5998; c) J. Zhou, B. He, B. Chen, P. Lu, H. H. Y. Sung, I. D. Williams, A. Qin, H. Qiu, Z. Zhao, B. Z. Tang, *Dyes Pigments* **2013**, *99*, 520.
[11] a) K. Tamao, M. Uchida, T. Izumizawa, K. Furukawa, S. Yamaguchi, *J. Am. Chem. Soc.* **1996**, *118*, 11974; b) S. Yamaguchi, T. Endo, M. Uchida, T. Izumizawa, K. Furukawa, K. Tamao, *Chem. Lett.* **2001**, *30*, 98; c) M. Uchida, T. Izumizawa, T. Nakano, S. Yamaguchi, K. Tamao, K. Furukawa, *Chem. Mater.* **2001**, *13*, 2680; d) H. Murata, Z. H. Kafafi, M. Uchida, *Appl. Phys. Lett.* **2002**, *80*, 189; e) W. Kim, L. C. Palilis, M. Uchida, Z. H. Kafafi, *Chem. Mater.* **2004**, *16*, 4681; f) H. Fu, Y. Cheng, *Curr. Org. Chem.* **2012**, *16*, 1423.
[12] L. C. Palilis, H. Murata, M. Uchida, Z. H. Kafafi, *Org. Electron.* **2003**, *4*, 113.
[13] a) H. Chen, W. Lam, J. Luo, Y. Ho, B. Z. Tang, D. Zhu, M. Wong, H. Kwok, *Appl. Phys. Lett.* **2002**, *81*, 574; b) Z. Zhao, S. Chen, J. W. Y. Lam, C. K. W. Jim, C. Y. K. Chan, Z. Wang, P. Lu, H. S. Kwok,

Y. Ma, B. Z. Tang, *J. Phys. Chem. C* **2010**, *114*, 7963; c) Z. Li, Y. Q. Dong, B. Mi, Y. Tang, M. Häußler, H. Tong, Y. P. Dong, J. W. Y. Lam, Y. Ren, H. H. Y. Sun, K. S. Wong, P. Gao, I. D. Williams, H. S. Kwok, B. Z. Tang, *J. Phys. Chem. B* **2005**, *109*, 10061; d) Z. Li, Y. Q. Dong, J. W. Y. Lam, J. Sun, A. Qin, M. Häußler, Y. P. Dong, H. H. Y. Sung, I. D. Williams, H. S. Kwok, B. Z. Tang, *Adv. Funct. Mater.* **2009**, *19*, 905; e) B. Chen, Y. Jiang, L. Chen, H. Nie, B. He, P. Lu, H. H. Y. Sung, I. D. Williams, H. S. Kwok, A. Qin, Z. Zhao, B. Z. Tang, *Chem. Eur. J.* **2014**, *20*, 1931.

- [14] a) W. L. Jia, M. J. Moran, Y.-Y. Yuan, Z. H. Lu, S. Wang, *J. Mater. Chem.* **2005**, *15*, 3326; b) D. Li, H. Zhang, C. Wang, S. Huang, J. Guo, Y. Wang, *J. Mater. Chem.* **2012**, *22*, 4319; c) X. Xu, S. Ye, B. He, B. Chen, J. Xiang, J. Zhou, P. Lu, Z. Zhao, H. Qiu, *Dyes Pigments* **2014**, *101*, 136.
- [15] T. Makino, R. Yamasaki, S. Saito, *Synthesis* **2008**, *72*, 859.
- [16] Z. Zhao, Z. Wang, P. Lu, C. Y. K. Chan, D. Liu, J. W. Y. Lam, H. H. Y. Sung, I. D. Williams, Y. Ma, B. Z. Tang, *Angew. Chem. Int. Ed.* **2009**, *48*, 7608.
- [17] a) H.-J. Son, W.-S. Han, J.-Y. Chun, C.-J. Lee, J.-I. Han, J. Ko, S. O. Kang, *Organometallics* **2007**, *26*, 519; b) T. Jiang, Y. Jiang, W. Qin, S. Chen, Y. Lu, J. W. Y. Lam, B. He, P. Lu, H. H. Y. Sung, I. D. Williams, H. S. Kwok, Z. Zhao, H. Qiu, B. Z. Tang, *J. Mater. Chem.* **2012**, *22*, 20266.
- [18] a) J. Xiao, H. Zhu, X. Wang, X. Gao, Z. Yang, X. Zhang, S. Wang, *J. Appl. Phys.* **2012**, *112*, 014513; b) Z. B. Wang, M. G. Helander, Z. W. Liu, M. T. Greiner, J. Qiu, Z. H. Lu, *Appl. Phys. Lett.* **2010**, *96*; c) Y. C. Zhou, J. Zhou, J. M. Zhao, S. T. Zhang, Y. Q. Zhan, X. Z. Wang, Y. Wu, X. M. Ding, X. Y. Hou, *Appl. Phys. A* **2006**, *83*, 465; d) V. Bulović, R. Deshpande, M. E. Thompson, S. R. Forrest, *Chem. Phys. Lett.* **1999**, *308*, 317; e) C. L. Chiang, S. M. Tseng, C. T. Chen, C. P. Hsu, C. F. Shu, *Adv. Funct. Mater.* **2008**, *18*, 248.
- [19] E. G. Wang, C. Li, W. L. Zhang, J. B. Peng, Y. Cao, *J. Mater. Chem.* **2008**, *18*, 797.
- [20] W. Z. Yuan, S. Chen, J. W. Y. Lam, C. Deng, P. Lu, H. H. Y. Sung, I. D. Williams, H. S. Kwok, Y. Zhang, B. Z. Tang, *Chem. Commun.* **2011**, *47*, 11216.
- [21] J. You, S.-L. Lai, W. Liu, T.-W. Ng, P. Wang, C.-S. Lee, *J. Mater. Chem.* **2012**, *22*, 8922.
- [22] P. A. Lane, G. P. Kushto, Z. H. Kafafi, *Appl. Phys. Lett.* **2007**, *90*, 023511.
- [23] J. Lee, Y.-Y. Yuan, Y. Kang, W.-L. Jia, Z.-H. Lu, S. Wang, *Adv. Funct. Mater.* **2006**, *16*, 681.